Acta Pharmaceutica Sinica B 2022;12(3):1288−1304

Chinese Pharmaceutical Association
Institute of Materia Medica, Chinese Academy of Medical Sciences

Acta Pharmaceutica Sinica B

www.elsevier.com/locate/apsb
www.sciencedirect.com

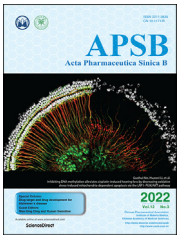

ORIGINAL ARTICLE

The FAPα-activated prodrug Z-GP-DAVLBH inhibits the growth and pulmonary metastasis of osteosarcoma cells by suppressing the AXL pathway

Geni Ye[a,b,†], Maohua Huang[a,b,c,†], Yong Li[a,b], Jie Ouyang[a,b], Minfeng Chen[a,b], Qing Wen[a,b], Xiaobo Li[a,b], Huhu Zeng[a,b], Pei Long[a,b], Zepei Fan[d], Junqiang Yin[d,*], Wencai Ye[a,b,*], Dongmei Zhang[a,b,*]

[a]*College of Pharmacy, Jinan University, Guangzhou 510632, China*
[b]*Guangdong Province Key Laboratory of Pharmacodynamic Constituents of Traditional Chinese Medicine and New Drugs Research, Jinan University, Guangzhou 510632, China*
[c]*Integrated Chinese and Western Medicine Postdoctoral Research Station, Jinan University, Guangzhou 510632, China*
[d]*Department of Musculoskeletal Oncology, the First Affiliated Hospital of Sun Yat-sen University, Guangzhou 510080, China*

Received 4 June 2021; received in revised form 27 July 2021; accepted 30 July 2021

KEY WORDS

Osteosarcoma;
Fibroblast activation protein alpha;
Growth;
Pulmonary metastasis;

Abstract Osteosarcoma is a kind of bone tumor with highly proliferative and invasive properties, a high incidence of pulmonary metastasis and a poor prognosis. Chemotherapy is the mainstay of treatment for osteosarcoma. Currently, there are no molecular targeted drugs approved for osteosarcoma treatment, particularly effective drugs for osteosarcoma with pulmonary metastases. It has been reported that fibroblast activation protein alpha (FAPα) is upregulated in osteosarcoma and critically associated with osteosarcoma progression and metastasis, demonstrating that FAPα-targeted agents might be a promising

Abbreviations: DAVLBH, desacetylvinblastine monohydrazide; EMT, epithelial−mesenchymal transition; FAPα, fibroblast activation protein alpha; siRNA, small interfering RNA; TA-MSCs, tumor-associated mesenchymal stem cells; Z-GP, N-terminal benzyloxy carbonyl-blocked (Z-blocked) GlyPro peptide; Z-GP-DAVLBH, desacetylvinblastine monohydrazide coupled to an N-terminal benzyloxy carbonyl-blocked (Z-blocked) GlyPro peptide.

*Corresponding authors. Tel.: +86 20 85222653, +86 20 85220004, +86 20 87755766.
E-mail addresses: dmzhang701@jnu.edu.cn (Dongmei Zhang), chywc@aliyun.com (Wencai Ye), yinjunq@mail.sysu.edu.cn (Junqiang Yin).
[†]These authors made equal contributions to this work.

Peer review under responsibility of Chinese Pharmaceutical Association and Institute of Materia Medica, Chinese Academy of Medical Sciences.

https://doi.org/10.1016/j.apsb.2021.08.015

Vinblastine prodrug;
AXL;
β-Catenin

therapeutic strategy for osteosarcoma. In the present study, we reported that the FAPα-activated vinblastine prodrug Z-GP-DAVLBH exhibited potent antitumor activities against FAPα-positive osteosarcoma cells *in vitro* and *in vivo*. Z-GP-DAVLBH inhibited the growth and induced the apoptosis of osteosarcoma cells. Importantly, it also decreased the migration and invasion capacities and reversed epithelial−mesenchymal transition (EMT) of osteosarcoma cells *in vitro* and suppressed pulmonary metastasis of osteosarcoma xenografts *in vivo*. Mechanistically, Z-GP-DAVLBH suppressed the AXL/AKT/GSK-3β/β-catenin pathway, leading to inhibition of the growth and metastatic spread of osteosarcoma cells. These findings demonstrate that Z-GP-DAVLBH is a promising agent for the treatment of FAPα-positive osteosarcoma, particularly osteosarcoma with pulmonary metastases.

1. Introduction

Osteosarcoma, the most frequent primary solid tumor of bone, is one of most commonly diagnosed malignancies in childhood and adolescence[1,2]. Osteosarcoma cells often exhibit highly and locally invasive growth and chemotherapy and/or radiotherapy are administered before or after surgery to inhibit tumor growth and metastatic spread[3]. The main therapy for osteosarcoma is surgery in combination with chemotherapy. Chemotherapeutic drugs typically include doxorubicin, cisplatin, and methotrexate[4–6]. However, these drugs are highly toxic to osteosarcoma patients and patients easily develop acquired resistance to chemotherapy[7], which is one of the key obstacles that limit the clinical benefits of these agents. Moreover, it has been disappointing that osteosarcoma patients only have obtained weak clinical benefits from oncogenic kinase-targeted therapy due to the high levels of genomic instability in osteosarcoma cells[8,9], leading to failure of the approval of molecular targeted drugs. Despite efforts to intensify the chemotherapeutic effects, osteosarcoma patients with distant metastases have a poor prognosis with a 5-year overall survival rate of less than 25%[3,6,8]. Pulmonary metastasis is a major malignant behavior of osteosarcoma cells[10] and the predominant cause of cancer-related death in osteosarcoma patients[3]. Currently, there are still no effective therapeutic agents for patients with metastatic osteosarcoma. Therefore, it is urgent to develop innovative and effective drugs for osteosarcoma patients with pulmonary metastases.

The AXL signaling pathway is hyperactivated in many kinds of cancers and is crucially implicated in tumor growth, epithelial−mesenchymal transition (EMT), and metastasis[11,12]. Some studies have reported that AXL is frequently upregulated in osteosarcoma tissues[13] and cell lines[14,15] and is closely associated with osteosarcoma growth and invasiveness[14–16]; thus, AXL is considered a potential therapeutic target in osteosarcoma[16,17]. Tumor EMT is a reversible biological program in which cells undergo a transition from an epithelial phenotype to a mesenchymal phenotype and it contributes to migration and metastasis in diverse types of malignancies[18,19]. Increasing evidence supports an important role of AXL in promoting EMT[11], and multiple studies have demonstrated that EMT is also critically related to osteosarcoma lung metastasis[20,21]. Thus, it is plausible that inhibiting AXL-mediated EMT is critical for the management of osteosarcoma metastasis.

Fibroblast activation protein alpha (FAPα), a type II transmembrane protein that belongs to the prolyl dipeptidyl aminopeptidase family, functions as a dipeptidyl peptidase that cleaves peptide substrates after a proline residue[22]. Previous studies revealed that FAPα was specifically overexpressed in tumor stromal cells, whereas, FAPα was also upregulated in certain types of cancers including osteosarcoma[23,24]. High expression of FAPα was significantly correlated with advanced clinical stage, high histological grade, positive metastatic status, and shorter overall and disease-free survival times in osteosarcoma patients[23], indicating that FAPα might be a promising therapeutic target for osteosarcoma. As reported, the FAPα-activated prodrug strategy has shown great potential for clinical application in cancer treatment[25,26]. Z-GP-DAVLBH, an FAPα-activated vinblastine prodrug that desacetylvinblastine monohydrazide (DAVLBH) was coupled to an N-terminal benzyloxy carbonyl-blocked (Z-blocked) GlyPro peptide (Z-GP), was synthesized by our group and it exhibited a potent antineoplastic activity in triple-negative breast cancer cell xenograft mouse models[26,27]. However, whether Z-GP-DAVLBH exerts antitumor effects on osteosarcoma cells and the mechanisms by which Z-GP-DAVLBH inhibits the aggressive progression of osteosarcoma remain largely uncharacterized.

In the present study, we found that the FAPα-activated prodrug Z-GP-DAVLBH suppressed the growth and metastasis of FAPα-positive osteosarcoma cells *in vitro* and *in vivo* by blocking the AXL/AKT/GSK-3β/β-catenin pathway. Our results indicate that Z-GP-DAVLBH has the potential to be developed as a new drug for the treatment of FAPα-positive osteosarcoma, particularly pulmonary metastatic osteosarcoma.

2. Materials and methods

2.1. Cells and cell culture

The human osteosarcoma cell lines SJSA-1 and 143B were obtained from the American Type Culture Collection (ATCC, Rockville, MD, USA). The U2-OS and MNNG/HOS cells were purchased from the Chinese Academy of Sciences Cell Bank (Shanghai, China). Osteosarcoma cells were grown in DMEM (Invitrogen, Waltham, MA, USA) supplemented with 10% FBS (ExCell Bio, Shanghai, China) and 1% penicillin−streptomycin (HyClone, Logan, UT, USA). Human brain vascular pericytes (HBVPs) were purchased from ScienCell Research Laboratories (San Diego, CA, USA) and cultured in Pericyte Medium containing 2% FBS, 1% pericyte growth supplement, and 1% penicillin−streptomycin. These cells were incubated in a humidified environment containing 5% CO_2 at 37 °C. Human immortalized

osteoblast hFOB 1.19 cells (Procell Life Science&Technology Co., Ltd.) were cultured in DMEM/F12 (Invitrogen) containing 0.3 mg/mL G418 (TargetMol, Boston, MA, USA) at 34 °C. The cells were routinely confirmed to be negative for mycoplasma.

2.2. *Hydrolysis of the prodrug mediated by FAPα-positive osteosarcoma cells in vitro*

Z-GP-DAVLBH and its parent drug DAVLBH (purity >98%) were synthesized according to previously described methods[26]. It was dissolved in DMSO (Sigma, St. Louis, MO, USA) to prepare a 20 mmol/L stock solution and was protected from light at −20 °C. The protocol for prodrug hydrolysis was performed according to a previous description[26]. Briefly, DAVLBH was first diluted in serum-free DEME medium at gradient concentrations from 20 to 0.3125 μmol/L and then was subjected to LC−MS analysis (Waters). 1 μmol/L vinblastine (Selleck Chemicals, Huston, TX, USA) was added and served as the internal standard. Data of ion peak of DAVLBH and vinblastine were collected. Then the standard curve was drawn with the ratios (the peak area of DAVLBH/the peak area of vinblastine) as *Y* axis and the concentrations of DAVLBH as *X* axis. Osteosarcoma cells and HBVPs (1.5×10^5) were placed in a 6-well plate and cultured overnight. The culture medium was replaced with serum-free DMEM containing 10 μmol/L Z-GP-DAVLBH with or without talabostat (TAL, Selleck Chemicals). The supernatants were collected after the cells were cultured for 2 h at 37 °C, centrifuged at 18,000×*g* for 15 min, and then the internal standard was added to each group. After filtration, the peak areas of DAVLBH were analyzed by LC−MS and the concentrations of DAVLBH were calculated according to the standard curve. The hydrolysis rate was equal to the concentrations of DAVLBH in each group/10 μmol/L × 100%.

2.3. *Cell viability assay*

The viability of SJSA-1,143B, U-2OS, and MNNG/HOS osteosarcoma cells was measured by an MTT assay. Briefly, cells (4×10^3 cells/well) were seeded in 96-well plates and cultured overnight. Then, the cells were treated with different concentrations of Z-GP-DAVLBH for 24, 48, and 72 h, respectively. The medium was discarded, and the cells were incubated with 5 mg/mL MTT (Sigma) at 37 °C for 2 h. Formazan was dissolved in DMSO and optical density was read in a microplate reader with a wavelength of 595 nm.

2.4. *Colony formation assay*

SJSA-1 and 143B cells were seeded in 6-well microplates at a density of 1.5×10^5 cells/well and cultured overnight. Then, the cells were treated with various concentrations of Z-GP-DAVLBH for 48 h and harvested by trypsinization (Gibco, Grand Island, NY, USA). Next, 600 cells were seeded in another 6-well plate and further cultured for 10 days. Cells were fixed with 4% paraformaldehyde (Sigma) at room temperature for 1 h and stained with 0.1% crystal violet (Sigma) for 20 min. Cell colonies were photographed under an inverted phase contrast microscope and the cell colonies were counted.

2.5. *Cell cycle analysis*

Osteosarcoma cells were treated with different concentrations of Z-GP-DAVLBH for the indicated times and then perform as previously described[28]. Firstly, the cells were collected and fixed in precooled 70% ethanol (Sigma) at 4 °C overnight. Then, the cells were further incubated with propidium iodide staining solution (Beyotime Biotechnology, Shanghai, China) containing 0.01 mg/mL PI and 0.1 mg/mL RNase A at 37 °C for 30 min in the dark. BD FACSCanto™ flow cytometer (BD Biosciences, CA, USA) was used to detect the red fluorescence at an excitation wavelength of 488 nm. The DNA contents were analyzed using ModFit LT 2.8 software (Becton Dickinson, CA, USA).

2.6. *Apoptosis assay*

The effect of Z-GP-DAVLBH on apoptosis was assessed with an Annexin-V-FITC/PI dual staining assay. Briefly, osteosarcoma cells (2×10^5) were seeded in 6-well plates and cultured overnight. Then, the cells were treated with Z-GP-DAVLBH for the indicated times. After treatment, the cells were harvested and stained with an Annexin V-FITC apoptosis detection kit (Beyotime Biotechnology) according to the manufacturer's protocol. The proportion of apoptotic cells was analyzed by BD FACSCanto™ Flow Cytometer.

2.7. *Measurement of mitochondrial membrane potential ($\Delta\Psi_m$)*

The effect of Z-GP-DAVLBH on the inner mitochondrial membrane potential ($\Delta\Psi_m$) in osteosarcoma cells was assessed by using the staining reagent JC-1. Briefly, osteosarcoma cells (2×10^5) were seeded in 6-well plates and cultured overnight. Then, the cells were treated with Z-GP-DAVLBH for the indicated times. After treatment, the cells were harvested and stained with a mitochondrial membrane potential assay kit with JC-1 (Beyotime Biotechnology) according to the manufacturer's protocol. The change in cellular fluorescence was analyzed by BD FACSCanto™ flow cytometer.

2.8. *Western blotting analysis*

For total protein extraction, osteosarcoma cells treated as indicated were washed twice with precooled PBS (HyClone) and lysed in ice-cold RIPA lysis buffer containing phosphatase inhibitor (Roche, Indianapolis, IN, USA), and protease inhibitor cocktail (Roche) for 30 min on ice. After centrifugation at 12,000×*g* and 4 °C for 15 min, the supernatants were collected and analyzed with a BCA Protein Assay Kit (Pierce, Rochford, IL, USA). Then, electrophoresis and immunoblot analysis were performed as previously described[29]. The proteins and color prestained protein marker (M221, GenStar, Beijing, China) were separated on sodium dodecyl sulfate-polyacrylamide gel electrophoresis (SDS-PAGE) gels and then transferred onto polyvinylidene fluoride membranes (Millipore). After blocking, the membranes were incubated with primary antibodies and then with anti-rabbit IgG and anti-mouse IgG. The following antibodies were used at a dilution of 1:500−1:1000: p-AXL (Tyr779) (catalog AF2228) and FAPα (catalog AF3715) were obtained from R&D system (Minneapolis, MN, USA). AXL (catalog 8661), p-AKT (Ser473) (catalog 4060), AKT (catalog 4691), p-histone H3 (Ser10) (catalog 53348), CDC2 (catalog 9116), CDC25C (5H9) (catalog 4688), CHK2 (catalog 3440), cyclin B1 (catalog 12231), Ki67 (catalog 9449), GAPDH (catalog 5174), E-cadherin (catalog 3195), N-cadherin (catalog 4061), ZO-1 (catalog 13663), Slug (catalog 9585), PARP (catalog 9532), cleaved PARP (catalog 5625), caspase-3 (catalog 14220), cleaved caspase-3 (catalog 9664), caspase-9 (catalog 9508), cleaved caspase-9

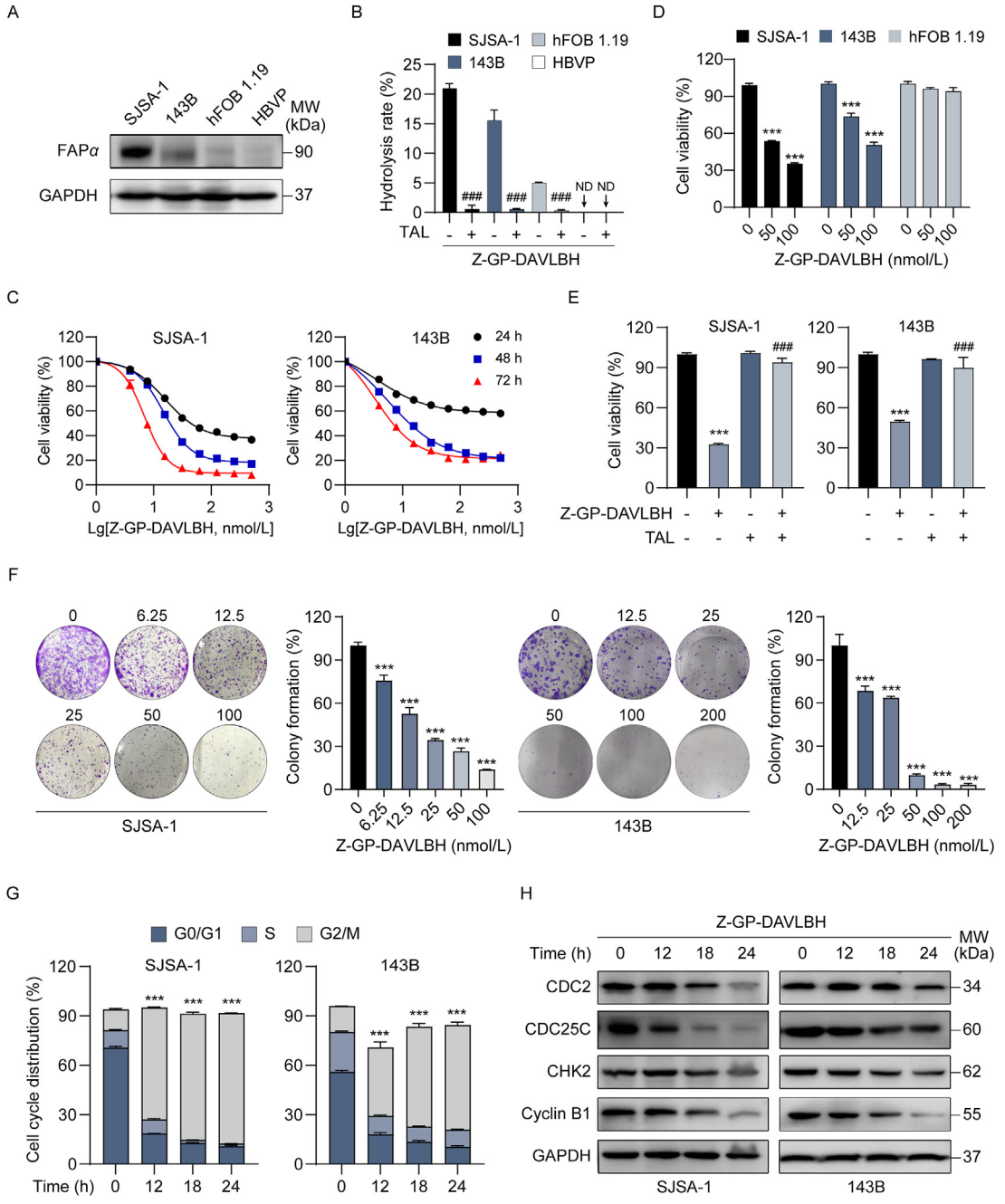

Figure 1 Z-GP-DAVLBH inhibits the proliferation of osteosarcoma cells *in vitro*. (A) The protein levels of FAPα in SJSA-1, 143B, hFOB 1.19 cells, and HBVPs were determined by Western blotting analysis. (B) SJSA-1, 143B, hFOB 1.19 cells, and HBVPs were treated with Z-GP-DAVLBH (10 μmol/L) in the presence or absence of TAL for 2 h. The hydrolysis efficiency of Z-GP-DAVLBH was analyzed by LC−MS. HBVPs serve as an FAPα-negative control cells. ND, no detection. (C) Osteosarcoma cells (SJSA-1 and 143B) were treated with various concentrations of Z-GP-DAVLBH for 24, 48, and 72 h. Cell viability was detected by an MTT assay. (D) MTT assay was conducted to determine the effect of Z-GP-DAVLBH on the viability of hFOB 1.19 cells. (E) Osteosarcoma cells (SJSA-1 and 143B) were treated with Z-GP-DAVLBH (50 nmol/L for SJSA-1 cells and 100 nmol/L for 143B cells) for 48 h in the presence or absence of TAL. Cell viability was detected by MTT assay. (F) Cell colony formation assay of SJSA-1 and 143B cells treated with the indicated concentrations of Z-GP-DAVLBH. Representative images of cell colonies are shown and clonogenicity was quantitated by normalization to the untreated group. Magnification: 100×. (G) The cell cycle distribution was detected by flow cytometry analysis. (H) Cell cycle-associated proteins were analyzed by Western blotting analysis. Data are presented as mean ± SEM, $n = 3$; $^{***}P<0.001$ *vs.* the untreated (0 nmol/L, 0.1% DMSO) group; $^{\#\#\#}P < 0.001$ *vs.* the Z-GP-DAVLBH-treated group.

(catalog 20750), GSK-3β (catalog 9315), p-GSK-3β (Ser9) (catalog 5558), β-catenin (catalog 8480), active β-catenin (catalog 8814), p-β-catenin (Ser552) (catalog 5651), and GAPDH (catalog 5174) were purchased from Cell Singling Technology (Danvers, MA, USA). Vimentin (catalog MA516409) was obtained from Invitrogen. All Western blotting analyses were performed at least three replications and the gray values of the protein bands were quantified with ImageJ software.

2.9. Cell adhesion assay

To assess cell adhesion ability, 96-well plates were precoated with 50 μg/mL human fibronectin (Corning, MA, USA) overnight at 4 °C. Osteosarcoma cells were pretreated with different concentrations of Z-GP-DAVLBH for 48 h. Then, the cells were harvested, and 5000 cells resuspended in 100 μL of serum-free DMEM were seeded into the precoated 96-well plates. After incubation at 37 °C for 2 h, the nonadherent cells were removed. The adherent cells were washed twice with PBS, fixed with 4% paraformaldehyde, and stained with 0.1% crystal violet. The number of cells adhered to the fibronectin was quantified with an inverted microscope.

2.10. Cell migration and invasion assay

The effect of Z-GP-DAVLBH on osteosarcoma cell migration and invasion was determined by a Transwell assay as previously described[30]. Briefly, osteosarcoma cells (2×10^4 cells/well) suspended in 100 μL of serum-free DMEM were seeded in the upper chambers of Transwell plate (24-well plate, 8-mm pore size, Corning). Then, 500 μL of DMEM containing 10% FBS and Z-GP-DAVLBH was added to the lower chambers. After culturing for 24 h, cells were fixed with 4% paraformaldehyde at room temperature for 30 min and stained with 0.1% crystal violet for 20 min. The non-migrated cells in the upper chambers were removed with a cotton swab. The cells in five random microscopic fields were photographed, and the number of migrated cells was quantified. For the Transwell invasion assay, the inserts in the upper chambers were precoated with 30 μL (2.5 mg/mL) of diluted Matrigel (Corning).

2.11. Quantitative real-time PCR

Total RNA was extracted using an E.Z.N.A. Total RNA Kit I (Omega Bio-Tek, USA) according to the manufacturer's protocol. Reverse transcription of total RNA was performed by using a Transcriptor First Strand cDNA Synthesis Kit (Bimake, Houston, TX, USA). Primers, SYBR Green I Master Mix (Bimake), and cDNA templates were mixed to generate the PCR system. qPCR was performed in a Roche LightCycler 480 real-time PCR instrument (Roche) with the following thermal cycling parameters: 45 cycles at 95 °C for 10 s, 60 °C for 20 s, and 72 °C for 20 s. The relative mRNA expression levels of the target genes were normalized to that of a housekeeping gene, *ACTB*, and the results were compared to those for the control group. Briefly, the $2^{-\Delta\Delta CT}$ method was used to calculate the relative amounts of mRNA. The primers were designed and synthesized by Sangon Biotech (Shanghai, China) and the sequences are listed in Supporting Information Table S1.

2.12. Cell transfection

For small interfering RNA (siRNA) transfection, osteosarcoma cells were transfected with the indicated siRNA duplexes or a negative control siRNA using Lipofectamine™ 3000 (Invitrogen). AXL was knocked down with the following siRNA duplexes: 5′-GGACAUAGGGCUAAGGCAATT-3′ and 5′-UUGCCUUAGCCCUAUGUCCTT-3′. A negative control siRNA duplex that did not target any gene product was used as a negative control, and its sequences were 5′-UUCUCCGAACGUGUCACGUTT-3′ and 5′-ACGUGACACGUUCGGAGAATT-3′. The siRNA duplexes were designed and synthesized by Sangon Biotech. For plasmid transfection, osteosarcoma cells were transfected with pFLAG AXL (Addgene plasmid # 105933; http://n2t.net/addgene:105933; RRID: Addgene_105933), IRES-GFP-AXL-KD (Addgene plasmid #65498; http://n2t.net/addgene:65498; RRID: Addgene_65498), and their corresponding empty vectors by Lipofectamine 3000™ reagent according to the manufacturer's protocol. After a 6-h transfection, the medium was refreshed and transfected cells were cultured for another 24 h before Z-GP-DAVLBH treatment.

2.13. Animal study

Four-to six-week-old male BALB/c nude mice were purchased from GemPharmatech Co., Ltd. (Nanjing, China). All animals were raised in an SPF environment with constant temperature and humidity and a 12-h light/dark cycle. In addition, all animal experimental procedures were conducted under the supervision of the Laboratory Animal Ethics Committee of Jinan University (Guangzhou, China) and adhered to the NIH Guide for the Care and Use of Laboratory Animals. The establishment of tumor xenografts and calculation of tumor volumes were performed as previously described[31]. Briefly, following anesthesia with 0.5 % pentobarbital sodium (i.p, 200 μL/mouse). 143B or SJSA-1 cells (4×10^7 cells/ml) suspended in PBS (50 μL/mice) were orthotopically injected with insulin syringes into the proximal end of the tibia of male BALB/c nude mice. When tumors grew to approximately 80 mm^3, the tumor-bearing mice were randomly divided into the vehicle or experimental group ($n = 6$ or 7). The tumor volumes were examined and calculated using Eq. (1):

$$\text{Tumor volume} = 4/3 \times \pi \times [1/4 \times (a+b)]^2 \quad (1)$$

where a refers to the longer diameter and b indicates the shorter diameter perpendicular to a[31]. Mice were administered with 2 mg/kg Z-GP-DAVLBH *via* intravenous injection every other day. After treatment for 20 days (SJSA-1 xenograft tumors) or 22 days (143B xenograft tumors), mice were euthanized, and tumor tissues were resected, weighed, and photographed. Then, primary tumor (containing tibias) and lung tissues were fixed, embedded, and sectioned, followed by histology and immunohistochemistry analyses.

2.14. Histology, immunohistochemistry, and immunofluorescence analyses

Tumors and lung tissues were fixed, embedded in paraffin, sectioned at a thickness of 5 μm, and then stained with H&E following standard procedures. Images were photographed by an

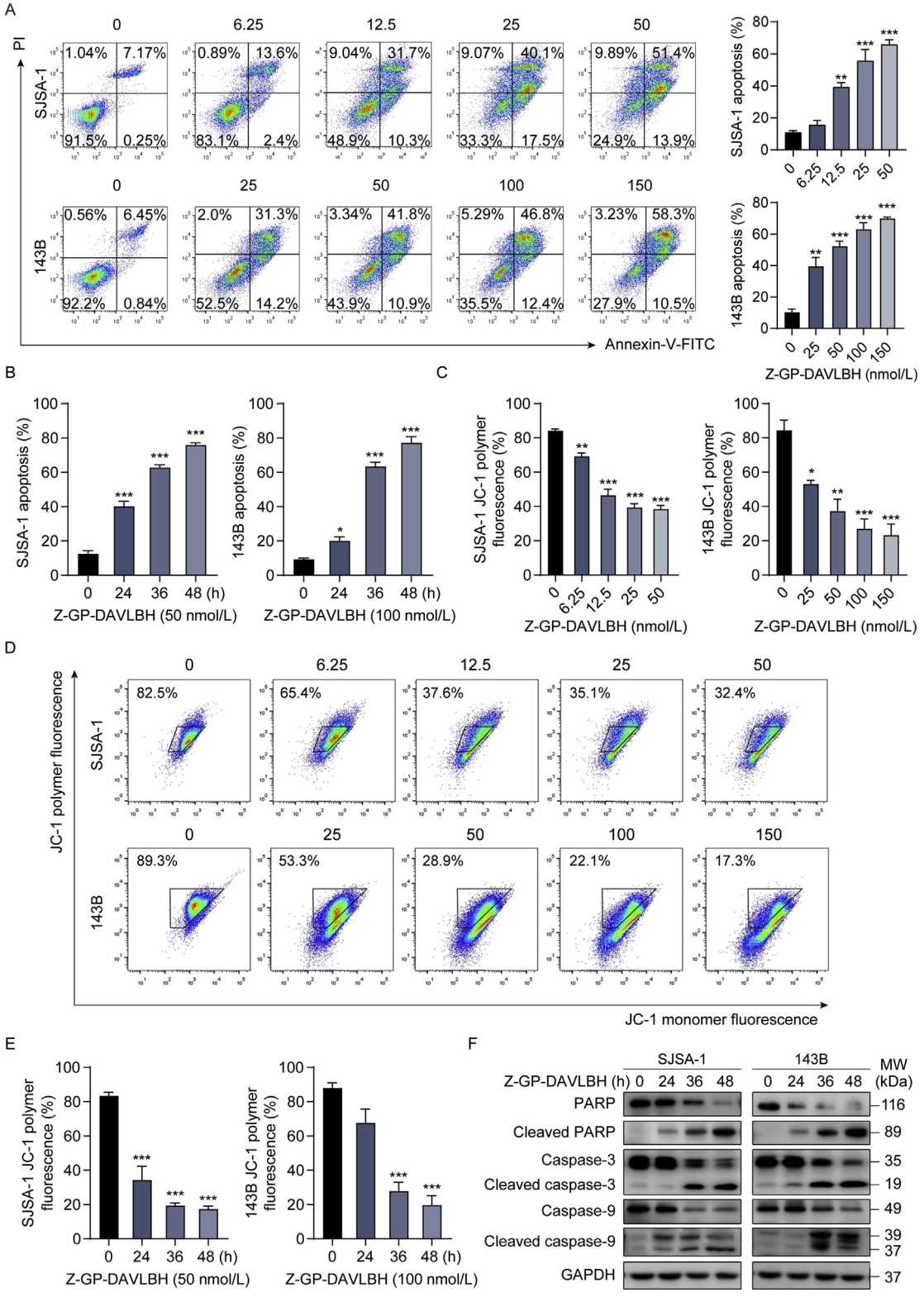

Figure 2 Z-GP-DAVLBH induces apoptosis in osteosarcoma cells. (A) and (B) Osteosarcoma cells (SJSA-1 and 143B) were (A) exposed to various concentrations of Z-GP-DAVLBH for 48 h, or (B) treated with Z-GP-DAVLBH for the indicated times. Apoptosis was examined with an Annexin V-FITC apoptosis detection kit. Representative flow cytometry plots and quantification of apoptotic cells. (C)−(E) Osteosarcoma cells (SJSA-1 and 143B) were (C) treated with Z-GP-DAVLBH for the indicated times or (D) incubated with gradient concentrations of Z-GP-DAVLBH for 48 h. Mitochondrial membrane potential (MMP) was assessed with a JC-1 kit. (E) Quantification of JC-1 polymer fluorescence of (D) is shown. (F) The expression of PARP, cleaved PARP, caspase-3, cleaved caspase-3, caspase 9, and cleaved caspase-9 in SJSA-1 and 143B cells were determined by Western blotting analysis. Representative blots are shown. Data are presented as mean±SEM, $n = 3$; $^{*}P<0.05$, $^{**}P<0.01$, and $^{***}P<0.001$ *vs.* the untreated (0 nmol/L, 0.1% DMSO) group.

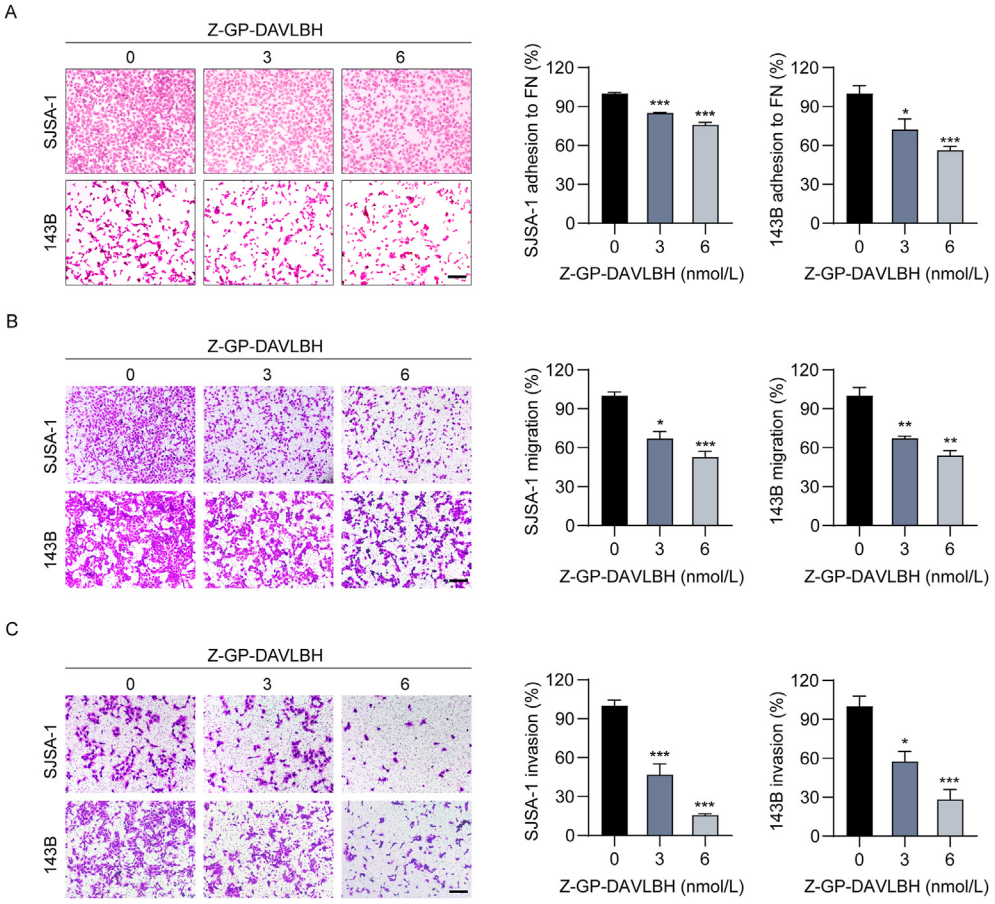

Figure 3 Z-GP-DAVLBH decreases the adhesion, migration, and invasion capacities of osteosarcoma cells. (A) Representative images of SJSA-1 and 143B cell adhered to fibronectin after treatment with Z-GP-DAVLBH. Quantification of the number of cells adhered to fibronectin. Scale bar, 200 μm. (B) and (C) The effect of Z-GP-DAVLBH on the migration and invasion of SJSA-1 and 143B cells was determined by Transwell (B) migration and (C) invasion assays. (B) Representative images and quantification of the number of migrated cells. Scale bar, 200 μm. (C) Representative images and quantification of the number of invaded cells. Scale bar, 200 μm. Data are presented as mean ± SEM, $n = 3$; *$P<0.05$, **$P<0.01$, and ***$P<0.001$ *vs.* the untreated (0 nmol/L, 0.1% DMSO) group.

inverted microscope (IX70, Olympus, Japan). The area and number of lung metastases were quantified with ImageJ software. For the quantification of the area of lung metastatic foci, the scale unit of H&E staining images was set to pixels/μm, the contours of lung metastatic foci were marked with freehand selections, and then the areas were analyzed and measured. The number of lung metastatic foci was counted with a multi-point tool. For immunohistochemical (IHC) staining, the sections were deparaffinized, dehydrated, and then treated with antigen retrieval. The slides were incubated with E-cadherin, ZO-1, vimentin, ZEB1, p-AXL, active β-catenin, Ki67, cleaved caspase-3, and p-histone H3 overnight at 4 °C, and then incubated with HRP-conjugated secondary antibodies and stained with a DAB kit (Pierce). Images were photographed by an inverted microscope. For immunofluorescence analysis, cells were fixed with 4% paraformaldehyde, blocked with 5% BSA (Sigma), permeabilized with 0.5% Triton X-100 (Sigma), and incubated with antibody against E-cadherin, ZO-1, vimentin, or ZEB1 overnight at 4 °C. Then, the cells were incubated with corresponding Alexa Fluor dye-conjugated secondary antibodies (Invitrogen) followed by nuclear staining with DAPI (Sigma). The images were captured by a laser scanning confocal microscope (LSM 800, ZEISS, Jena, Germany). The quantifications of IHC and immunofluorescence staining were performed using ImageJ software.

2.15. *Statistical analysis*

All *in vitro* experiments were conducted at least three independent replicates. Data were presented as mean ± standard error of mean (SEM) values, and statistical analyses were performed with GraphPad Prism 7.0 software (GraphPad Software, Inc., San Diego, CA, USA). The significance of differences was assessed using an unpaired two-tailed *t*-test (for two groups) or one-way with ANOVA and Tukey's multiple comparison test (for more than two groups). $P<0.05$ indicated a significant difference.

3. Results

3.1. *Z-GP-DAVLBH is hydrolyzed by FAPα-positive osteosarcoma cells and inhibits their proliferation in vitro*

Since FAPα is highly expressed in human osteosarcoma tissues and critically implicated in osteosarcoma development and

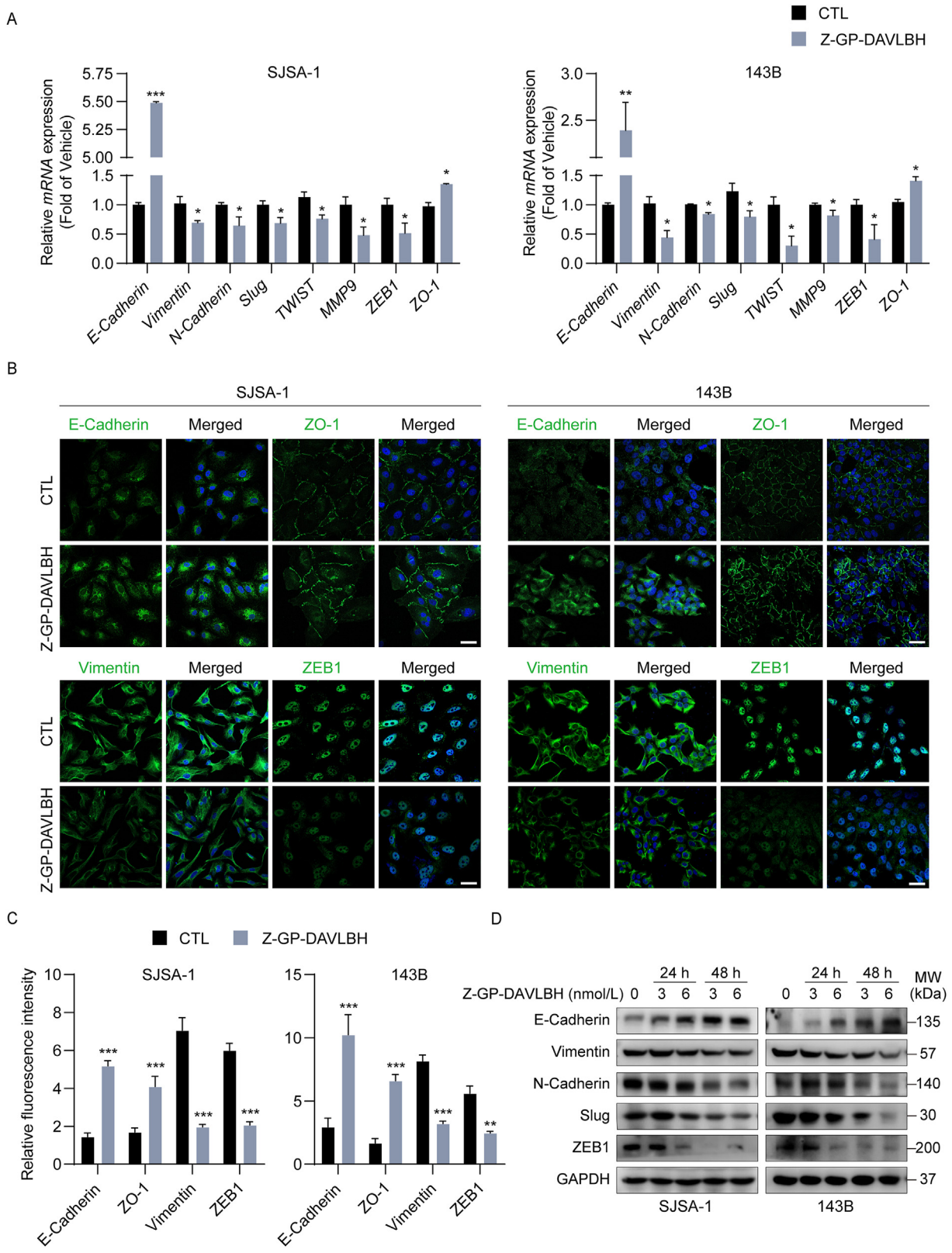

Figure 4 Z-GP-DAVLBH impairs epithelial−mesenchymal transition in osteosarcoma cells. (A) SJSA-1 and 143B cells were treated with Z-GP-DAVLBH (6 nmol/L) for 48 h, and the relative mRNA expression levels of EMT-related genes were determined by RT-PCR assay. (B) SJSA-1 and 143B cells were treated with Z-GP-DAVLBH (6 nmol/L) for 48 h, and the expression of vimentin, ZEB-1, E-cadherin, and ZO-1 was evaluated by immunofluorescence staining analysis. Scale bar: 50 μm. (C) Quantification of relative fluorescence intensity in (B) is shown. (D) Osteosarcoma cells were treated with Z-GP-DAVLBH (3 or 6 nmol/L) for 24 and 48 h and then the expression of EMT-related markers was determined by Western blotting assay. Data are presented as mean±SEM, $n = 3$; *$P<0.05$, **$P<0.01$, and ***$P<0.001$ *vs.* the CTL (0.1% DMSO) group.

progression[23−26], we first determined the expression of FAPα in human osteoblasts and osteosarcoma cells. FAPα was significantly upregulated in human osteosarcoma SJSA-1 and 143B cells compared to human immortalized osteoblast hFOB1.19 cells (Fig. 1A). Then, FAPα-positive osteosarcoma cells and osteoblasts were incubated with Z-GP-DAVLBH and their hydrolytic properties were determined. Our results showed that Z-GP-DAVLBH was hydrolyzed by FAPα-positive osteosarcoma cells, among which SJSA-1 cells with the highest expression of FAPα showed a higher hydrolytic rate than 143B and hFOB1.19 cells (Fig. 1B). Pretreatment of osteosarcoma cells with TAL, a selective inhibitor of FAPα, completely blocked the hydrolytic effect of FAPα-positive osteosarcoma cells (Fig. 1B). Osteosarcoma cells with low expression of FAPα showed a decreased capacity to hydrolyzed Z-GP-DAVLBP (Supporting Information Fig. S1A and S1B). These differences demonstrated that Z-GP-DAVLBH was specifically hydrolyzed by FAPα in osteosarcoma cells. Next, the antitumor effects of Z-GP-DAVLBH on FAPα-positive osteosarcoma cell lines were assessed. Z-GP-DAVLBH significantly decreased the viability of SJSA-1 and 143B cells in a concentration-dependent manner (Fig. 1C). Z-GP-DAVLBH also dramatically reduced the viability of U2-OS and MNNG/HOS cells (Supporting Information Fig. S2). We also found that the IC_{50} values of Z-GP-DAVLBH in SJSA-1 and 143B cells were dramatically lower than those of doxorubicin and cisplatin, two commonly used chemotherapeutic drugs in the clinical treatment of osteosarcoma (Supporting Information Table S2). The IC_{50} values (72 h) of Z-GP-DAVLBH, doxorubicin, and cisplatin for SJSA-1 cells were 55.3±8.2, 322.0±7.4, and 2410.0±89.8 nmol/L, respectively. Those for 143B cells were 112.0±8.1, 2650.0±3.3, and 3020.5±72.3 nmol/L, respectively. Moreover, we found that Z-GP-DAVLBH showed a slight effect on hFOB1.19 cell viability, compared to SJSA-1 and 143B cells (Fig. 1D). Inhibition of FAPα using TAL abrogated the ability of Z-GP-DAVLBH to decrease the cell viability of SJSA-1 and 143 cells (Fig. 1E). We also found that Z-GP-DAVLBH showed an attenuated ability to inhibit the viability of osteosarcoma cells with low expression of FAPα (Fig. S1C). Additionally, SJSA-1 and 143B cells incubated with Z-GP-DAVLBH also exhibited a significant reduction in clonogenicity, as determined by colony formation assay (Fig. 1F). Z-GP-DAVLBH induced cell cycle arrest at the G2/M phase in a time-dependent (Fig. 1G and H and Supporting Information Fig. S3A) and dose-dependent (Fig. S3B−S3D) manner. Together, these data suggest that Z-GP-DAVLBH effectively inhibits growth and induces cell cycle arrest in FAPα-positive osteosarcoma cells.

3.2. *Z-GP-DAVLBH induces apoptosis in osteosarcoma cells*

Then, we evaluated the ability of Z-GP-DAVLBH to induce apoptosis in osteosarcoma cells. Flow cytometric analysis shows that Z-GP-DAVLBH treatment markedly induced the apoptosis of SJSA-1 and 143B cells in a dose-dependent (Fig. 2A) and time-dependent (Fig. 2B) manner. Since loss of the inner mitochondrial transmembrane potential ($\Delta\Psi_m$) in cells is a characteristic of apoptosis, we further investigated whether Z-GP-DAVLBH damaged mitochondria by a JC-1 staining kit. The decrease in JC-1 polymer fluorescence indicates loss of $\Delta\Psi_m$ in cells. After treatment with Z-GP-DAVLBH, we found that the proportion of cells with JC-1 polymer fluorescence was substantially decreased in a dose- (Fig. 2C and D) and time-dependent (Fig. 2E) manner. Additionally, Z-GP-DAVLBH induced specific cleavage of PARP and activation of caspase-9 and caspase-3 in SJSA-1 and 143B cells (Fig. 2F and Supporting Information Fig. S4). Taken together, our results indicate that Z-GP-DAVLBH elicits mitochondrial apoptosis in osteosarcoma cells.

3.3. *Z-GP-DAVLBH decreases the adhesion and mobility capacities of osteosarcoma cells in vitro*

High invasiveness is an aggressive malignant behavior of osteosarcoma cells[10]. Therefore, we further explored the effect of Z-GP-DAVLBH on the adhesion and mobility of osteosarcoma cells *in vitro*. With a moderate inhibitive effect on cell viability (Supporting Information Fig. S5), we found that Z-GP-DAVLBH treatment significantly decreased the abilities of SJSA-1 and 143B cells to adhere to fibronectin (Fig. 3A). Furthermore, Transwell assays showed that Z-GP-DAVLBH treatment significantly reduced the number of migrated SJSA-1 and 143B cells in a concentration-dependent manner (Fig. 3B). The invasiveness of osteosarcoma cells was considerably attenuated after incubation with Z-GP-DAVLBH (Fig. 3C). Together, these findings reveal that Z-GP-DAVLBH suppresses the adhesion, migration, and invasion of osteosarcoma cells *in vitro*.

3.4. *Z-GP-DAVLBH inhibits epithelial−mesenchymal transition in osteosarcoma cells*

Given that tumor cell EMT critically contributes to tumor migration and metastasis, we next assessed whether Z-GP-DAVLBH had a suppressive effect on EMT in osteosarcoma cells. EMT is characterized by loss of epithelial makers, including E-cadherin and ZO-1, and upregulation of mesenchymal markers, such as N-cadherin, Vimentin, Slug, Twist1, and ZEB1. We found that Z-GP-DAVLBH treatment appreciably increased the expression of epithelial markers and led to a dramatic reduction in the expression of mesenchymal makers in SJSA-1 and 143B cells, as measured by RT-PCR (Fig. 4A) and cell immunofluorescence assays (Fig. 4B and C). Moreover, Western blotting analysis showed that Z-GP-DAVLBH treatment increased the expression of the epithelial marker E-cadherin, but decreased the expression of mesenchymal markers including N-cadherin, Vimentin, Slug, and ZEB1 in osteosarcoma cells (Fig. 4D and Supporting Information Fig. S6). Taken together, these results indicate that Z-GP-DAVLBH inhibits EMT in osteosarcoma cells.

3.5. *Z-GP-DAVLBH suppresses the AXL/AKT/GSK-3β/β-catenin pathway in osteosarcoma cells*

Then, we further investigated the mechanisms by which Z-GP-DAVLBH inhibited the aggressive malignant phenotypes of osteosarcoma cells. Numerous studies have reported that AXL is critically implicated in tumor cell growth, metastasis, invasion, and EMT[11,32]. Thus, we next determined the effect of Z-GP-DAVLBH on the AXL pathway in osteosarcoma cells. We found that Z-GP-DAVLBH significantly decreased the levels of p-AXL (Tyr779), p-AKT (Ser473), and p-GSK-3β (Ser9) in SJSA-1 and 143B cells (Fig. 5A and Supporting Information Fig. S7A). AKT phosphorylates β-catenin at Ser552[33] and increased phosphorylated GSK-3β leads to a decrease in β-catenin phosphorylation at Ser33, Ser37, and Thr41[34,35], which promotes the stabilization and nuclear translocation of β-catenin and subsequently enhances the

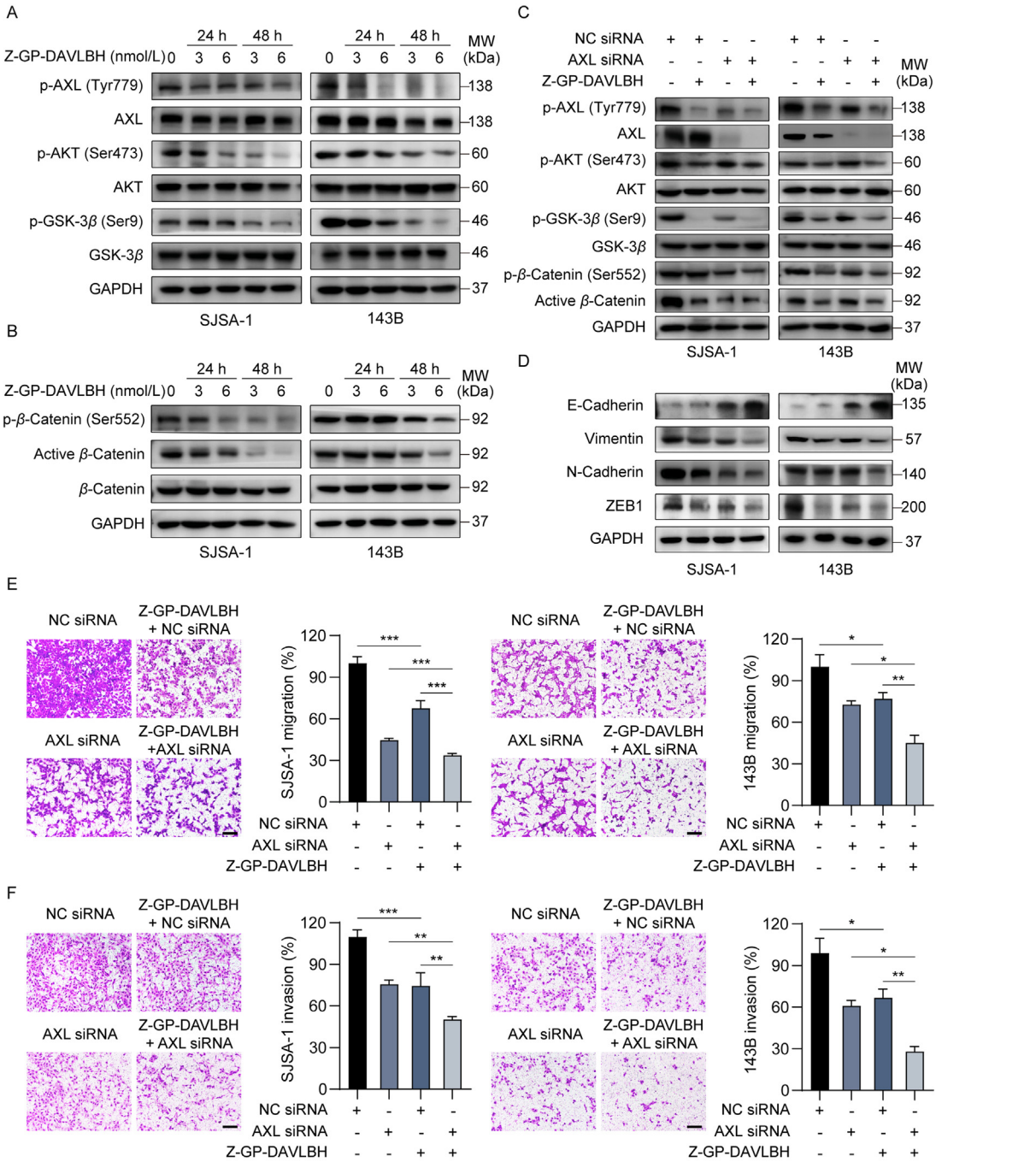

Figure 5 Z-GP-DAVLBH inhibits the AXL/AKT/GSK-3β/β-catenin pathway in osteosarcoma cells. (A)−(B) Osteosarcoma cells were treated with vehicle (0.1% DMSO) or Z-GP-DAVLBH (6 nmol/L) for 48 h. (A) The levels of p-AXL (Tyr779), AXL, p-AKT (Ser473), AKT, p-GSK-3β (Ser9), and GSK-3β in SJSA-1 and 143B cells treated with Z-GP-DAVLBH were determined by Western blotting analysis. (B) Representative blots of β-catenin, β-catenin (Ser552), and non-phosphorylated (active) β-catenin (Ser33/37/Thr41) in osteosarcoma cells. (C) and (D) Osteosarcoma cells after transfection with either NC siRNA or AXL siRNA were treated vehicle (0.1% DMSO) or Z-GP-DAVLBH (6 nmol/L) for 48 h. (C) Western blotting analysis was conducted to evaluate the effect of Z-GP-DAVLBH on the AXL/AKT/GSK-3β/β-catenin pathway components and (D) EMT-related markers in osteosarcoma cells. (E) and (F) Osteosarcoma cells were treated with Z-GP-DAVLBH (6 nmol/L) for 24 h. Transwell assays were conducted to evaluate the effect of Z-GP-DAVLBH on the (E) migration and (F) invasion capacities of SJSA-1 and 143B cells transfected with the indicated siRNAs. Scale bar: 200 μm. Data are presented as mean±SEM, $n = 3$; *$P<0.05$, **$P<0.01$, and ***$P<0.001$ *vs.* the indicated groups.

transcriptional activity of β-catenin. As expected, Z-GP-DAVLBH treatment considerably reduced the level of β-catenin (Ser552) and active β-catenin in SJSA-1 and 143B cells (Fig. 5B and Fig. S7B). PCR analysis further confirmed that Z-GP-DAVLBH treatment downregulated β-catenin target genes in osteosarcoma cells (Supporting Information Fig. S8). These data suggest that Z-GP-DAVLBH inhibits the activation of the AXL/AKT/GSK-3β/β-catenin pathway in osteosarcoma cells.

3.6. AXL is responsible for Z-GP-DAVLBH-induced inhibition of growth and metastasis in osteosarcoma cells

We further identified the role of AXL in Z-GP-DAVLBH-mediated suppression of the growth and malignant behaviors in osteosarcoma cells. SJSA-1 and 143B cells were transfected with either NC or AXL siRNAs (Supporting Information Fig. S9A). Compared to Z-GP-DAVLBH treatment alone, Z-GP-DAVLBH treatment plus AXL silencing more potently decreased the levels of p-AXL (Tyr779), p-AKT (Ser473), and p-GSK-3β (Ser9) in SJSA-1 and 143B cells (Fig. 5C and Fig. S9B). Consequently, the expression of β-catenin (Ser552) and active β-catenin in osteosarcoma cells after Z-GP-DAVLBH treatment plus AXL silencing was much lower than that in osteosarcoma cells treated with Z-GP-DAVLBH alone (Fig. 5C and Fig. S9B). We also found that silencing AXL promoted the effect of Z-GP-DAVLBH on inhibiting EMT in osteosarcoma cells (Fig. 5D and Fig. S9C). Moreover, knockdown of AXL partially attenuated the migration and invasion abilities of SJSA-1 and 143B cells and the effect was further enhanced by Z-GP-DAVLBH treatment (Fig. 5E and F). The MTT assay and apoptosis assay confirmed that treatment with Z-GP-DAVLBH in combination with AXL siRNA more potently decreased the viability of osteosarcoma cells (Supporting Information Fig. S10A) and induced their apoptosis (Fig. S10B).

To further confirm the important role of AXL in Z-GP-DAVLBH-mediated inhibition of the growth and malignant behaviors of osteosarcoma cells, SJSA-1 and 143B cells were transfected either an AXL overexpression plasmid or an AXL overexpression plasmid with a kinase-dead AXL mutant (AXL-KD) (Supporting Information Fig. S11A). Western blotting analysis showed that ectopic expression of AXL reduced the ability of Z-GP-DAVLBH to inhibit the AXL/AKT/GSK-3β/β-catenin pathway (Fig. 6A and Fig. S11B) and EMT (Fig. 6B and Fig. S11C) in osteosarcoma cells. Compared to vector transfection, overexpression of AXL significantly promoted the mobility and viability, but attenuated the ability of Z-GP-DAVLBH to reduce the migration and invasion capacities and viability of osteosarcoma cells (Fig. 6C and D). Additionally, Z-GP-DAVLBH exhibited a weaker ability to induce apoptosis in AXL-overexpressing cells than in osteosarcoma cells transfected with vector or AXL-KD plasmid (Fig. 6E and Fig. S11D). However, the inhibitory effects of Z-GP-DAVLBH on the malignant behaviors of osteosarcoma cells transfected with AXL-KD were similar to those in cells transfected with corresponding empty vector (Fig. 6A–D and Fig. S11). These differences indicated that Z-GP-DAVLBH-mediated inhibition of AXL kinase activity was critical for the decreased malignant behaviors of osteosarcoma cells. Together, these results demonstrate that Z-GP-DAVLBH inhibits the aggressive malignant behaviors of osteosarcoma cells by suppressing the AXL/AKT/GSK-3β/β-catenin pathway.

3.7. Z-GP-DAVLBH suppresses the growth of xenografted osteosarcoma cells in vivo

Subsequently, we investigated the antineoplastic effects of Z-GP-DAVLBH in BALB/c nude mice bearing SJSA-1 or 143B cell xenografts. Based on previous studies[26,36], tumor-bearing mice received intravenous injection of Z-GP-DAVLBH (2.0 mg/kg) every other day. We found that both the average tumor volume (Fig. 7A, left panel) and average tumor weight (Fig. 7A, right panel) were appreciably decreased in mice treated with Z-GP-DAVLBH. Importantly, there was no significant loss of body weight in tumor-bearing mice after Z-GP-DAVLBH treatment (Fig. 7B). IHC staining and immunofluorescence assays further demonstrated dramatic decreases in the Ki67-and p-histone H3 (Ser10)-stained areas and a significant increase in the cleaved caspase-3-stained areas in osteosarcoma tumors upon Z-GP-DAVLBH treatment (Fig. 7C and D). Collectively, these observations suggest that Z-GP-DAVLBH inhibits the growth and induces the apoptosis of osteosarcoma cells *in vivo*.

3.8. Z-GP-DAVLBH inhibits epithelial–mesenchymal transition and prevents pulmonary metastasis of osteosarcoma cells in vivo

Finally, we evaluated the antimetastatic effect of Z-GP-DAVLBH in osteosarcoma orthotopic xenograft models by using histological and immunohistochemical analyses. Compared to vehicle group, Z-GP-DAVLBH treatment significantly decreased the number and the area of lung metastatic foci formed by 143B cells (Fig. 8A and B). Furthermore, we also confirmed that Z-GP-DAVLBH inhibited the lung metastasis of osteosarcoma cells by inhibiting AXL-mediated EMT. Our results show that Z-GP-DAVLBH treatment appreciably reversed EMT in orthotopic osteosarcoma xenograft tumors, as indicated by significant increases in ZO-1 and E-cadherin staining densities and dramatic decreases in ZEB1 and vimentin staining densities (Fig. 8C). Remarkably, Z-GP-DAVLBH considerably reduced the staining areas of p-AXL (Tyr779) and active β-catenin in osteosarcoma xenograft tumors (Fig. 8D). Collectively, our findings demonstrate that Z-GP-DAVLBH reverses EMT and suppresses the pulmonary metastasis of osteosarcoma cells *in vivo*.

4. Discussion

Osteosarcoma is a common type of aggressive bone tumor that mainly originates from mesenchymal tissues[1,2]. Currently, surgery is still the mainstay of osteosarcoma treatment and approximately 70% of osteosarcoma patients can be cured by surgical resection in combination with chemotherapy (doxorubicin and cisplatin with or without methotrexate)[8]. The majority of osteosarcoma patients have non-metastatic osteosarcoma, with a 5-year overall survival rate of up to 70%[37,38]. Although combined treatment with surgery and chemotherapy has provided great clinical benefits to osteosarcoma patients, patients with metastatic osteosarcoma have a 5-year overall survival rate of approximately 20%. Because in many osteosarcoma patients, lung metastasis has already occurred at the time of diagnosis[6,8,39]. Therefore, new therapies for lung metastatic osteosarcoma are urgently needed. In the present study, we found that the vinblastine derivative Z-GP-DAVLBH suppressed osteosarcoma cell proliferation, migration, invasion, and EMT, and induced their apoptosis. It also considerably inhibited growth and lung metastasis in the osteosarcoma xenograft mouse model by suppressing the AXL/AKT/GSK-3β/β-catenin pathway.

The AXL pathway is critically implicated in multiple malignant cell behaviors, such as tumor cell survival, growth, migration, invasion, EMT, drug resistance, and stem cell maintenance, in various types cancer[11,12]. AXL-mediated malignant phenotypes are mainly associated with the PI3K/AKT/mTOR, RAS/RAF/MEK/ERK, JAK/STAT, and NF-κB pathways[11,40]. EMT has a crucial relation with increased capacities for tumor cell migration and metastasis[18,41]. Currently, various signaling pathways have been confirmed to be critically associated with EMT, including the WNT/β-catenin and TGF/Smad pathways[42,43]. In addition to WNT ligands, many oncogenic kinases are related to β-catenin activation, which indicates that the β-catenin pathway can be activated in a WNT ligand-independent manner. Accumulating evidence has demonstrated that AXL triggers the activation of the β-catenin pathway *via* phosphorylation β-catenin

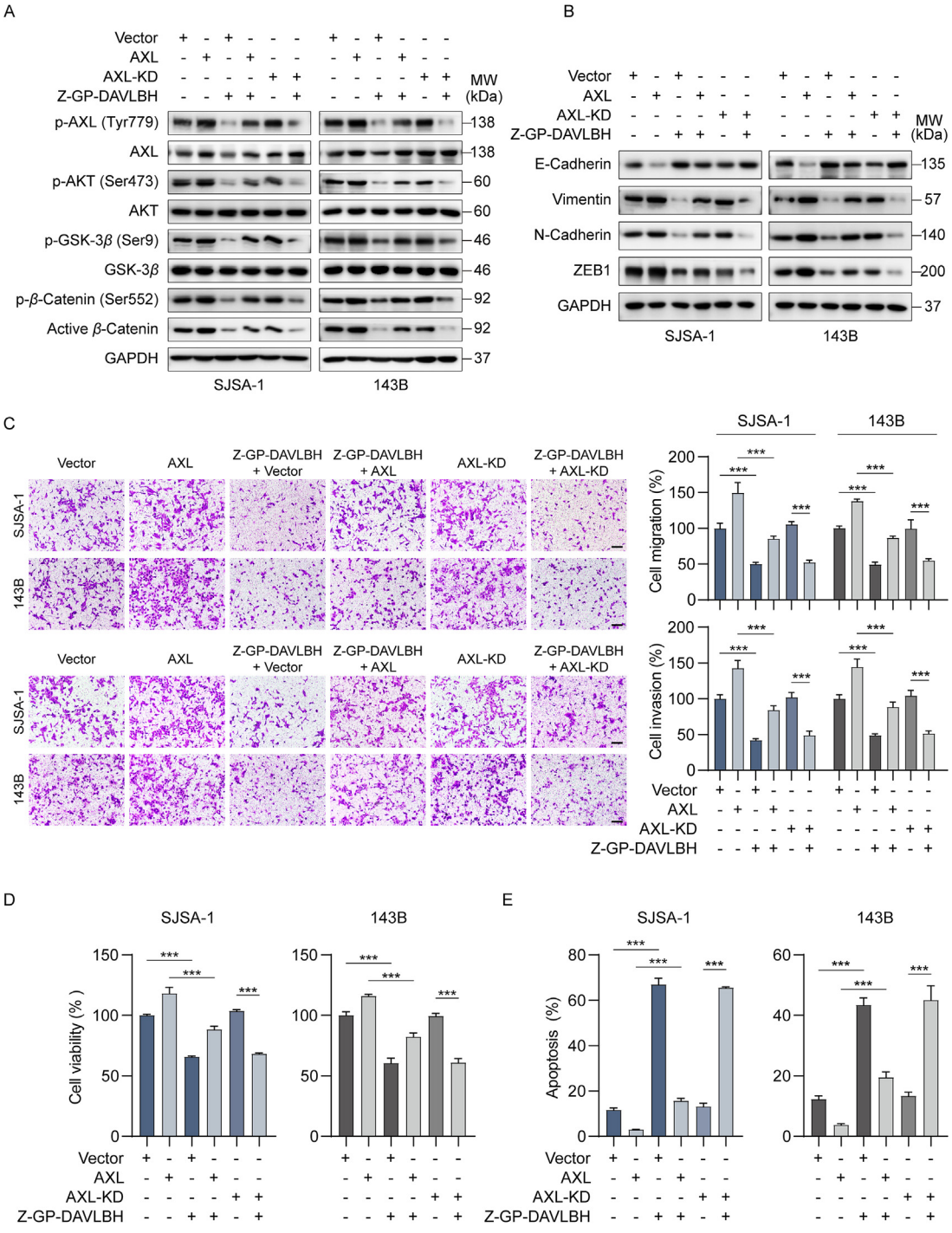

Figure 6 Ectopic expression of AXL attenuates the effect of Z-GP-DAVLBH on the malignant behaviors of osteosarcoma cells. (A) and (B) Osteosarcoma cells were treated with vehicle (0.1% DMSO) or Z-GP-DAVLBH (6 nmol/L) for 48 h. (A) Western blotting analysis of p-AXL (Tyr779), AXL, p-AKT (Ser473), AKT, p-GSK-3β (Ser9), GSK-3β, β-catenin, p-β-catenin (Ser552), and non-phosphorylated (active) β-catenin (Ser33/37/Thr41), and (B) EMT-related markers in SJSA-1 and 143B cells. (C) Osteosarcoma cells were treated with Z-GP-DAVLBH (6 nmol/L) for 24 h. Representative image of migrated (upper) and invaded (lower) osteosarcoma cells. Scale bar: 200 μm. Quantification of the number of migrated and invaded cells is shown. (D) and (E) SJSA-1 and 143B were treated with vehicle (0.1% DMSO) or Z-GP-DAVLBH (50 nmol/L for SJSA-1 cells and 100 nmol/L for 143B cells) for 48 h. (D) An MTT assay was conducted to evaluate the effect of Z-GP-DAVLBH on osteosarcoma cell viability. (E) An Annexin V-FITC apoptosis detection kit was used to evaluate the effect of Z-GP-DAVLBH on osteosarcoma cell apoptosis. Data are presented as mean±SEM, $n = 3$; *P<0.05, **P<0.01, and ***P<0.001 *vs.* the indicated group.

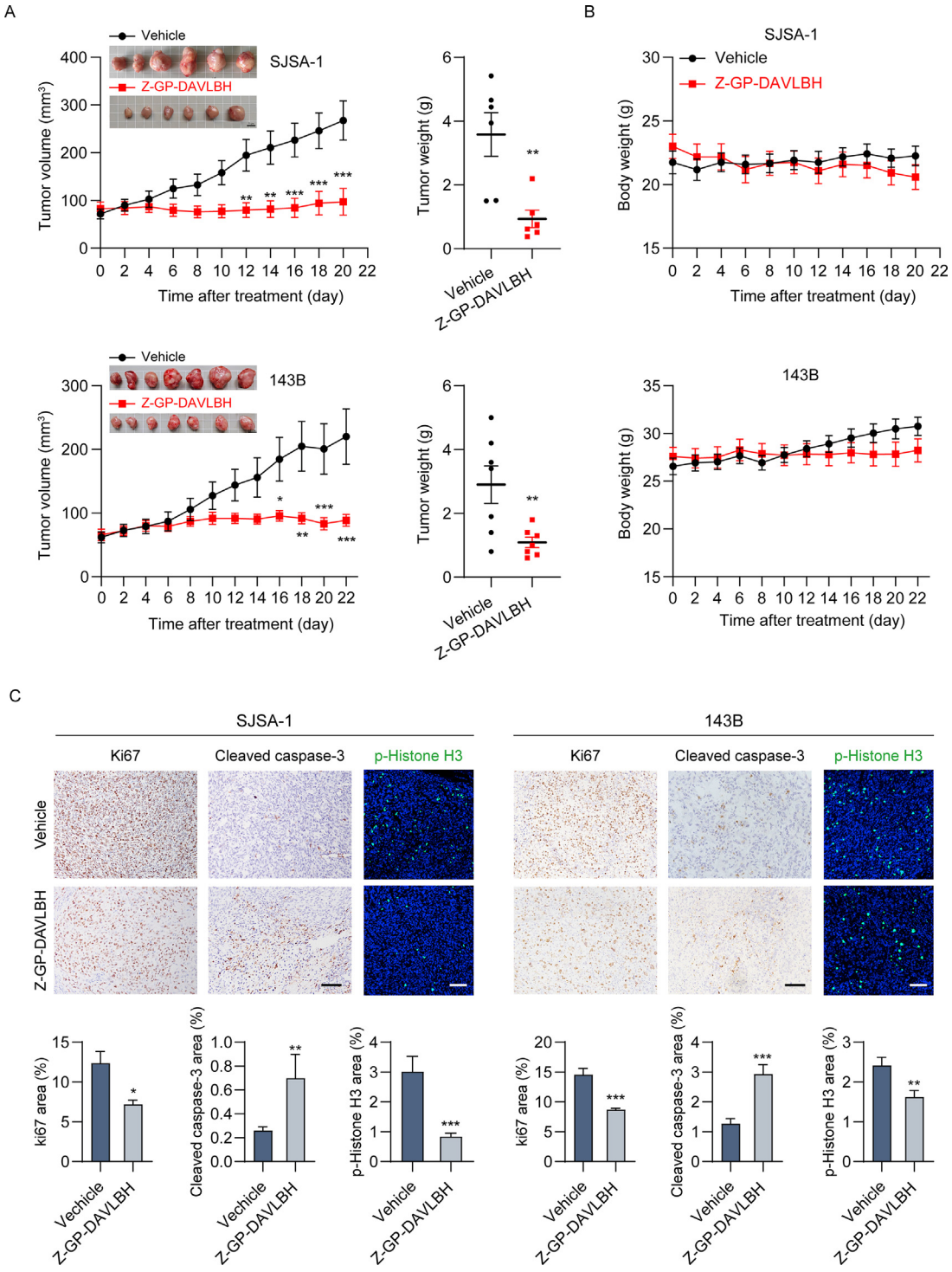

Figure 7 Z-GP-DABLBH suppresses the outgrowth of xenografted osteosarcoma cells in BALB/c nude mice. (A) and (B) BALB/c nude mice bearing SJSA-1 or 143B tumors were treated with vehicle (0.9% NaCl solution containing 1% DMSO) or Z-GP-DAVLBH (2 mg/kg, i.v.) every other day. The tumor volumes of tumor-bearing mice were measured every other day. (A, right) The weights of SJSA-1 and 143B tumors is shown. Representative images of tumors are shown. Scale bar: 1 cm. (B) The body weights of tumor bearing mice were measured every other day. (C) IHC staining of Ki67 and cleaved caspase-3 and immunofluorescence staining of p-histone H3 (Ser 10) in SJSA-1 and 143B xenograft tumors. Scale bar: 100 μm for IF images or 200 μm for IHC images. (D) Quantification of IHC and IF staining in tumor tissues. Data are presented as mean±SEM, $n = 6$ or 7; *$P<0.05$, **$P<0.01$, and ***$P<0.001$ *vs.* the Vehicle group.

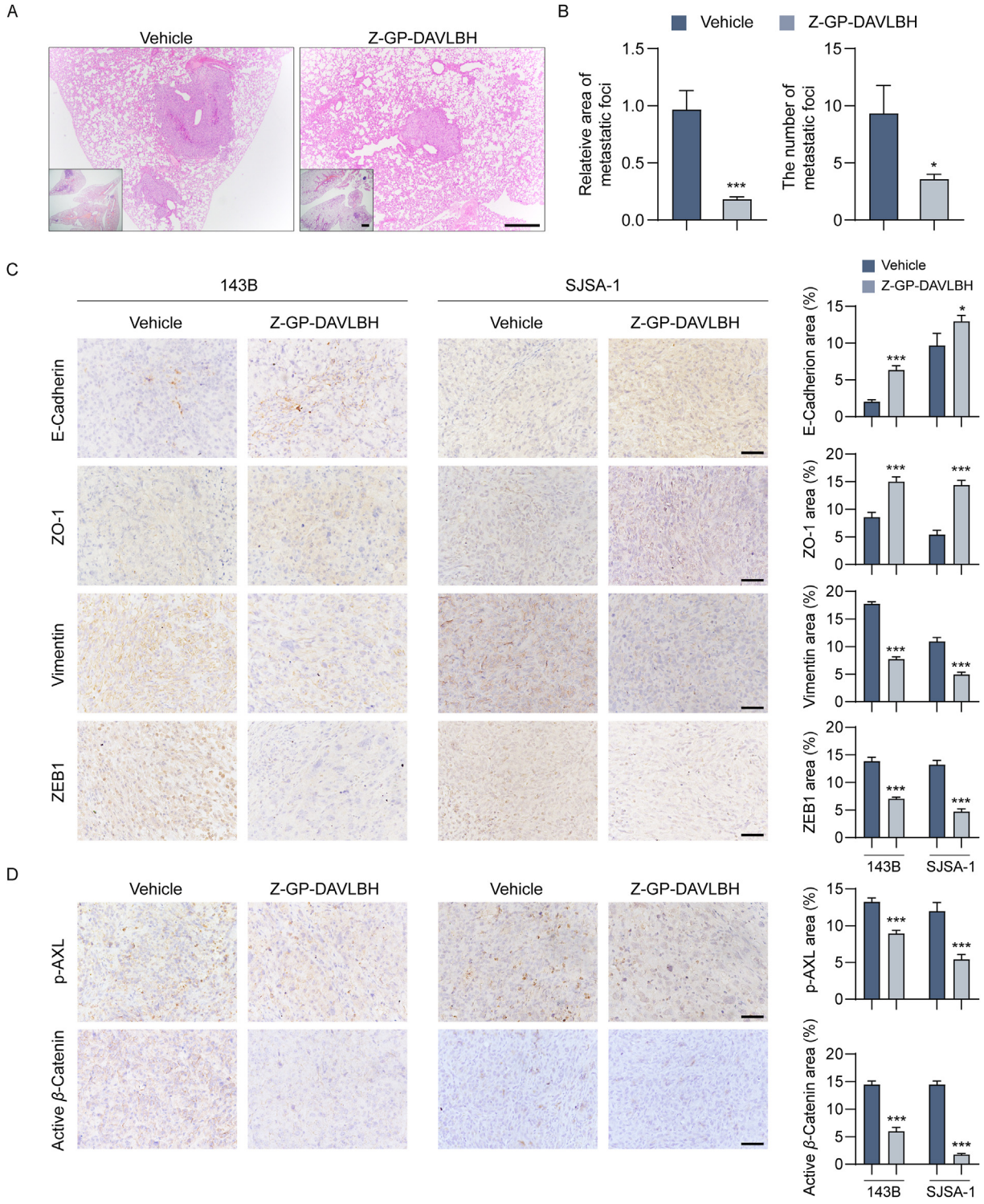

Figure 8 Z-GP-DAVLBH inhibits epithelial−mesenchymal transition and suppresses pulmonary metastasis of osteosarcoma cells *in vivo*. (A) BALB/c nude mice bearing 143B tumors were treated with vehicle (0.9% NaCl solution containing 1% DMSO) or Z-GP-DAVLBH (2 mg/kg, i.v.) every other day for 22 days. Lung tissues were collected and performed by hematoxylin-eosin (H&E) staining. Scale bar: 500 μm for low magnification images or 100 μm for high magnification images. (B) Quantification of the area and number of lung metastatic foci. (C) IHC staining of EMT-related markers in SJSA-1 and 143B tumor tissues. Quantification of IHC staining of EMT-related markers is shown. (D) IHC staining of p-AXL (Tyr779) and non-phosphorylated (active) β-catenin (Ser33/37/Thr41) in SJSA-1 and 143B tumor tissues. Scale bar: 50 μm. Quantification of IHC staining is shown. Data are presented as mean±SEM, $n = 6$; *$P<0.05$, **$P<0.01$, ***$P<0.001$ *vs.* the Vehicle group.

at Ser552 by AKT or/and dephosphorylation of β-catenin at Ser33/37/Thr41 in an AKT/GSK-3β-dependent manner[44,45]. For instance, AXL can promote the chemoresistance and metastasis of breast cancer cells[45], and enhance the self-renewal of chronic myelogenous leukemia stem cells[44] by enhancing the expression of β-catenin target genes. In our study, we found that Z-GP-DAVLBH can inhibit the AXL/AKT/GSK-3β/β-catenin pathway in osteosarcoma cells, as indicated by the significant decreases in the levels of phosphorylated AXL (Tyr779), AKT (Ser473), p-GSK-3β (Ser9), β-catenin (Ser552), and non-phosphorylated (active) β-catenin (Ser33/37/Thr41). We also observed that silencing AXL promoted but ectopic expression of AXL attenuated the antineoplastic effects of Z-GP-DAVLBH on osteosarcoma cells. Additionally, Z-GP-DAVLBH treatment led to a considerable decrease in the expression of β-catenin target genes in SJSA-1 and 143B cells. Our study indicates that Z-GP-DAVLBH may be a promising and effective therapeutic agent for osteosarcoma and suggests that the AXL/β-catenin axis could be a potential therapeutic target in osteosarcoma.

Based on the proteolytic activity of FAPα in the tumor microenvironment, many peptide-based cytotoxic prodrugs have been investigated in animal studies. FAPα-activated thapsigargin prodrugs are cleaved by FAPα-expressing cancer-associated fibroblasts and show a strong ability to inhibit the growth of MCF-7 and LNCaP xenograft tumors though selectively inducing the death of cancer-associated fibroblasts[25]. Z-GP-DAVLBH can be hydrolyzed by FAPα-positive pericytes to release the parent drug DAVLBH, which is accumulated in FAPα-positive pericytes and thus induces the destruction of tumor vasculatures, blocking tumor growth[26]. Compared to DAVLBH and vinblastine, Z-GP-DAVLBH exhibits a better anticancer effect and less toxicity in tumor-bearing mice[26], which indicates that FAPα-activated prodrug strategy facilitates the targeting of DAVLBH and vinblastine to the FAPα-positive cells. In addition to tumor pericytes and cancer-associated fibroblasts, Z-GP-DAVLBH can be cleaved by tumor-associated mesenchymal stem cells with FAPα expression (FAPα$^+$ TA-MSCs) in the tumor microenvironment. Consequently, it induces the apoptosis of FAPα$^+$ TA-MSCs and leads to a reduction in FAPα$^+$ TA-MSC-mediated pulmonary metastasis in triple-negative breast cancer mouse models[27]. Vinblastine and its derivatives exert broad-spectrum anticancer effects and also show potent antineoplastic effects on osteosarcoma cells *in vitro*[46], in mouse models[47], and in clinic treatment[48,49]. Moreover, FAPα is upregulated in human osteosarcoma cells, which suggested that Z-GP-DAVLBH might be activated by and then targeted FAPα-positive osteosarcoma cells. Herein, we found that Z-GP-DAVLBH was hydrolyzed by FAPα-positive osteosarcoma cells and that appreciably inhibited the aggressive malignant behaviors of osteosarcoma cells *in vitro* and *in vivo*. *In vivo* study also showed that Z-GP-DAVLBH had a negligible effect on FAPα expression in osteosarcoma xenograft tumors, indicating that FAPα acted as a hydrolytic enzyme rather than a therapeutic target of Z-GP-DAVLBH (Supporting Information Fig. S12). Our study reports for the first time that FAPα-activated prodrug strategy can be a potent and potential therapeutic strategy for treating metastatic osteosarcoma.

The antimetastatic effect of Z-GP-DAVLBH *in vivo* might be complex. In our *in vitro* experiments, Z-GP-DABLH (3 and 6 nmol/L) significantly inhibited the migration and invasion, and reversed EMT with a moderate effect on the viability of osteosarcoma cells. These results indicated that Z-GP-DABLH-induced inhibition of mobility and EMT was not caused by decreased viability *in vitro*. In our *in vivo* studies, we found that Z-GP-DAVLBH reversed the EMT in xenograft tumors, which might be critically responsible for a dramatic decrease in pulmonary metastasis. Besides, Z-GP-DAVLBH inhibited the growth and increased the apoptosis of osteosarcoma xenograft tumors, which may contribute to the antimetastatic effect *in vivo*.

5. Conclusions

In summary, our study demonstrates that Z-GP-DAVLBH has considerable antiproliferative and antimetastatic effects on osteosarcoma cells *in vitro* and *in vivo*. Z-GP-DAVLBH inhibits the growth, EMT, and pulmonary metastasis of osteosarcoma cells by suppressing the AXL/AKT/GSK-3β/β-catenin pathway. Our findings shed new light on the mechanisms underlying the antineoplastic activity of Z-GP-DAVLBH and demonstrate that a clinical trial of Z-GP-DAVLBH for the treatment of patients with pulmonary metastatic osteosarcoma is warranted.

Acknowledgments

This work was supported by National Natural Science Foundation of China (grant numbers: 82003796, 81803566, 81973340 and 81630095); Local Innovative and Research Teams Project of the Guangdong Pearl River Talents Program (grant number: 2017BT01Y036, China); National High-level Personnel of the Special Support Program (DM Zhang, China); National Science and Technology Major Project (grant number: 2018ZX09711001-008-008, China); Key-Area Research and Development Program of Guangdong Province (grant number: 2020B1111110004, China); Natural Science Foundation of Guangdong Province (grant number: 2019A1515010144, China); Guangdong Province Key Laboratory of Pharmacodynamic Constituents of TCM and New Drugs Research, College of Pharmacy (grant number: 2020B1212060076, China); Special Funds for the Cultivation of Guangdong College Students' Scientific and Technological Innovation (grant number: pdjh2021a0052, China).

Author contributions

Dongmei Zhang and Wencai Ye designed and supervised the experiments and revised the manuscript. Junqiang Yin provided critical reading and revision of the manuscript. Geni Ye and Maohua Huang wrote the manuscript and analyzed the data. Geni Ye, Yong Li, Jie Ouyang, Minfeng Chen, and Xiaobo Li performed animal experiments. Geni Ye and Qing Wen performed flow cytometry analysis and analyzed the data. Geni Ye and Maohua Huang performed immunofluorescence assay and image acquisition. Geni Ye, Maohua Huang, Qing Wen, and Zepei Fan performed cell line studies and Western blotting assay. Huhu Zeng performed LC/MS analysis.

Conflicts of interest

The authors declare that there are no conflicts of interest.

Appendix A. Supporting information

Supporting data to this article can be found online at https://doi.org/10.1016/j.apsb.2021.08.015.

References

1. Mirabello L, Troisi RJ, Savage SA. International osteosarcoma incidence patterns in children and adolescents, middle ages and elderly persons. *Int J Cancer* 2009;**125**:229−34.
2. Mirabello L, Troisi RJ, Savage SA. Osteosarcoma incidence and survival rates from 1973 to 2004: data from the surveillance, epidemiology, and end results program. *Cancer* 2009;**115**:1531−43.
3. Yang Z, Li X, Yang Y, He Z, Qu X, Zhang Y. Long noncoding RNAs in the progression, metastasis, and prognosis of osteosarcoma. *Cell Death Dis* 2016;**7**:e2389.
4. Meyers PA, Schwartz CL, Krailo M, Kleinerman ES, Betcher D, Bernstein ML, et al. Osteosarcoma: a randomized, prospective trial of the addition of ifosfamide and/or muramyl tripeptide to cisplatin, doxorubicin, and high-dose methotrexate. *J Clin Oncol* 2005;**23**:2004−11.
5. Whelan JS, Bielack SS, Marina N, Smeland S, Jovic G, Hook JM, et al. EURAMOS-1, an international randomised study for osteosarcoma: results from pre-randomisation treatment. *Ann Oncol* 2015;**26**:407−14.
6. Gill J, Ahluwalia MK, Geller D, Gorlick R. New targets and approaches in osteosarcoma. *Pharmacol Ther* 2013;**137**:89−99.
7. Zhu KP, Zhang CL, Ma XL, Hu JP, Cai T, Zhang L. Analyzing the interactions of mRNAs and ncRNAs to predict competing endogenous RNA networks in osteosarcoma chemo-resistance. *Mol Ther* 2019;**27**:518−30.
8. Kansara M, Teng MW, Smyth MJ, Thomas DM. Translational biology of osteosarcoma. *Nat Rev Cancer* 2014;**14**:722−35.
9. Brown HK, Tellez-Gabriel M, Heymann D. Cancer stem cells in osteosarcoma. *Cancer Lett* 2017;**386**:189−95.
10. Fan TM, Roberts RD, Lizardo MM. Understanding and modeling metastasis biology to improve therapeutic strategies for combating osteosarcoma progression. *Front Oncol* 2020;**10**:13.
11. Zhu C, Wei Y, Wei X. AXL receptor tyrosine kinase as a promising anti-cancer approach: functions, molecular mechanisms and clinical applications. *Mol Cancer* 2019;**18**:153.
12. Li Y, Ye X, Tan C, Hongo JA, Zha J, Liu J, et al. Axl as a potential therapeutic target in cancer: role of Axl in tumor growth, metastasis and angiogenesis. *Oncogenesis* 2009;**28**:3442−55.
13. Rettew AN, Young ED, Lev DC, Kleinerman ES, Abdul-Karim FW, Getty PJ, et al. Multiple receptor tyrosine kinases promote the *in vitro* phenotype of metastatic human osteosarcoma cell lines. *Oncogenesis* 2012;**1**:e34.
14. Nakano T, Tani M, Ishibashi Y, Kimura K, Park YB, Imaizumi N, et al. Biological properties and gene expression associated with metastatic potential of human osteosarcoma. *Clin Exp Metastasis* 2003;**20**:665−74.
15. Han J, Tian R, Yong B, Luo C, Tan P, Shen J, et al. Gas6/Axl mediates tumor cell apoptosis, migration and invasion and predicts the clinical outcome of osteosarcoma patients. *Biochem Biophys Res Commun* 2013;**435**:493−500.
16. Greenfield EM, Collier CD, Getty PJ. Receptor tyrosine kinases in osteosarcoma: 2019 update. *Adv Exp Med Biol* 2020;**1258**:141−55.
17. Tian Z, Niu X, Yao W. Receptor tyrosine kinases in osteosarcoma treatment: which is the key target?. *Front Oncol* 2020;**10**:1642.
18. Lu W, Kang Y. Epithelial-mesenchymal plasticity in cancer progression and metastasis. *Dev Cell* 2019;**49**:361−74.
19. Chaffer CL, San Juan BP, Lim E, Weinberg RA. EMT, cell plasticity and metastasis. *Cancer Metastasis Rev* 2016;**35**:645−54.
20. Han Y, Guo W, Ren T, Huang Y, Wang S, Liu K, et al. Tumor-associated macrophages promote lung metastasis and induce epithelial-mesenchymal transition in osteosarcoma by activating the COX-2/STAT3 axis. *Cancer Lett* 2019;**440**−**441**:116−25.
21. Liu W, Liu P, Gao H, Wang X, Yan M. Long non-coding RNA PGM5-AS1 promotes epithelial−mesenchymal transition, invasion and metastasis of osteosarcoma cells by impairing miR-140-5p-mediated FBN1 inhibition. *Mol Oncol* 2020;**14**:2660−77.
22. Yu DM, Yao TW, Chowdhury S, Nadvi NA, Osborne B, Church WB, et al. The dipeptidyl peptidase IV family in cancer and cell biology. *FEBS J* 2010;**277**:1126−44.
23. Yuan D, Liu B, Liu K, Zhu G, Dai Z, Xie Y. Overexpression of fibroblast activation protein and its clinical implications in patients with osteosarcoma. *J Surg Oncol* 2013;**108**:157−62.
24. Zhang L, Yang L, Xia ZW, Yang SC, Li WH, Liu B, et al. The role of fibroblast activation protein in progression and development of osteosarcoma cells. *Clin Exp Med* 2020;**20**:121−30.
25. Brennen WN, Rosen DM, Wang H, Isaacs JT, Denmeade SR. Targeting carcinoma-associated fibroblasts within the tumor stroma with a fibroblast activation protein-activated prodrug. *J Natl Cancer Inst* 2012;**104**:1320−34.
26. Chen M, Lei X, Shi C, Huang M, Li X, Wu B, et al. Pericyte-targeting prodrug overcomes tumor resistance to vascular disrupting agents. *J Clin Invest* 2017;**127**:3689−701.
27. Li X, Chen M, Lu W, Tang J, Deng L, Wen Q, et al. Targeting FAPα-expressing tumor-associated mesenchymal stromal cells inhibits triple-negative breast cancer pulmonary metastasis. *Cancer Lett* 2021;**503**:32−42.
28. Zhu L, Wang J, Kong W, Huang J, Dong B, Huang Y, et al. LSD1 inhibition suppresses the growth of clear cell renal cell carcinoma *via* upregulating P21 signaling. *Acta Pharm Sin B* 2019;**9**:324−34.
29. Sun H, Huang M, Yao N, Hu J, Li Y, Chen L, et al. The cycloartane triterpenoid ADCX impairs autophagic degradation through Akt overactivation and promotes apoptotic cell death in multidrug-resistant HepG2/ADM cells. *Biochem Pharmacol* 2017;**146**:87−100.
30. Chen L, Mai W, Chen M, Hu J, Zhuo Z, Lei X, et al. Arenobufagin inhibits prostate cancer epithelial−mesenchymal transition and metastasis by down-regulating β-catenin. *Pharmacol Res* 2017;**123**:130−42.
31. Berlin O, Samid D, Donthineni-Rao R, Akeson W, Amiel D, Woods Jr VL. Development of a novel spontaneous metastasis model of human osteosarcoma transplanted orthotopically into bone of athymic mice. *Cancer Res* 1993;**53**:4890−5.
32. Graham DK, DeRyckere D, Davies KD, Earp HS. The TAM family: phosphatidylserine sensing receptor tyrosine kinases gone awry in cancer. *Nat Rev Cancer* 2014;**14**:769−85.
33. Fang D, Hawke D, Zheng Y, Xia Y, Meisenhelder J, Nika H, et al. Phosphorylation of beta-catenin by AKT promotes beta-catenin transcriptional activity. *J Biol Chem* 2007;**282**:11221−9.
34. Yost C, Torres M, Miller JR, Huang E, Kimelman D, Moon RT. The axis-inducing activity, stability, and subcellular distribution of beta-catenin is regulated in *Xenopus* embryos by glycogen synthase kinase 3. *Genes Dev* 1996;**10**:1443−54.
35. Xu Z, Zhou Z, Zhang J, Xuan F, Fan M, Zhou D, et al. Targeting BMI-1-mediated epithelial−mesenchymal transition to inhibit colorectal cancer liver metastasis. *Acta Pharm Sin B* 2021;**11**:1274−85.
36. Lei X, Chen M, Li X, Huang M, Nie Q, Ma N, et al. A vascular disrupting agent overcomes tumor multidrug resistance by skewing macrophage polarity toward the M1 phenotype. *Cancer Lett* 2018;**418**:239−49.
37. Collins M, Wilhelm M, Conyers R, Herschtal A, Whelan J, Bielack S, et al. Benefits and adverse events in younger *versus* older patients receiving neoadjuvant chemotherapy for osteosarcoma: findings from a meta-analysis. *J Clin Oncol* 2013;**31**:2303−12.
38. Bernthal NM, Federman N, Eilber FR, Nelson SD, Eckardt JJ, Eilber FC, et al. Long-term results (>25 years) of a randomized, prospective clinical trial evaluating chemotherapy in patients with high-grade, operable osteosarcoma. *Cancer* 2012;**118**:5888−93.
39. Klein MJ, Siegal GP. Osteosarcoma: anatomic and histologic variants. *Am J Clin Pathol* 2006;**125**:555−81.
40. Linger RM, Keating AK, Earp HS, Graham DK. TAM receptor tyrosine kinases: biologic functions, signaling, and potential therapeutic targeting in human cancer. *Adv Cancer Res* 2008;**100**:35−83.
41. Pastushenko I, Blanpain C. EMT transition states during tumor progression and metastasis. *Trends Cell Biol* 2019;**29**:212−26.
42. Gonzalez DM, Medici D. Signaling mechanisms of the epithelial−mesenchymal transition. *Sci Signal* 2014;**7**:re8.

43. Shibue T, Weinberg RA. EMT, CSCs, and drug resistance: the mechanistic link and clinical implications. *Nat Rev Clin Oncol* 2017;**14**:611−29.
44. Wang C, Jin H, Wang N, Fan S, Wang Y, Zhang Y, et al. Gas6/Axl axis contributes to chemoresistance and metastasis in breast cancer through Akt/GSK-3β/β-catenin signaling. *Theranostics* 2016;**6**:1205−19.
45. Jin Y, Nie D, Li J, Du X, Lu Y, Li Y, et al. Gas6/AXL signaling regulates self-renewal of chronic myelogenous leukemia stem cells by stabilizing β-catenin. *Clin Cancer Res* 2017;**23**:2842−55.
46. Russo AJ, Magro PG, Hu Z, Li WW, Peters R, Mandola J, et al. E2F-1 overexpression in U2OS cells increases cyclin B1 levels and CDC2 kinase activity and sensitizes cells to antimitotic agents. *Cancer Res* 2006;**66**:7253−60.
47. Nakamura T, Kitagawa T. Anticancer drug screening test with LDH in nude mouse bearing bone and soft part sarcoma. *Cancer* 1985;**56**:1112−6.
48. Philip T, Iliescu C, Demaille MC, Pacquement H, Gentet JC, Krakowski I, et al. High-dose methotrexate and HELP [Holoxan (ifosfamide), eldesine (vindesine), platinum]—doxorubicin in non-metastatic osteosarcoma of the extremity: a French multicentre pilot study. Fédération Nationale des Centres de Lutte contre le Cancer and Société Française d'Oncologie Pédiatrique. *Ann Oncol* 1999;**10**:1065−71.
49. Souhami RL, Craft AW, Van der Eijken JW, Nooij M, Spooner D, Bramwell VH, et al. Randomised trial of two regimens of chemotherapy in operable osteosarcoma: a study of the European Osteosarcoma Intergroup. *Lancet* 1997;**350**:911−7.